Physica **60** (1972) 357–374 © *North-Holland Publishing Co.*

INELASTIC ENERGY LOSSES IN SMALL-ANGLE SCATTERING OF ENERGETIC PARTICLES

D.J. BIERMAN and W.C. TURKENBURG

FOM-Instituut voor Atoom- en Molecuulfysica, Amsterdam, Nederland

and

C.P. BHALLA

Kansas State University, Manhattan, Kansas, USA

Received 19 October 1971

Synopsis

Measurements are presented of inelastic energy losses, Q, dissipated in scattering events between a range of elements as projectiles and the noble-gas atoms neon and argon as target particles. Scattering angles are in the range between 10′ and 140′. The velocity of all the projectiles is 4.38×10^7 cm/s. Oscillations in Q as a function of the atomic number of the primary ion, are observed. The experimental values are compared with calculations based upon the semiclassical modified Firsov theory. The qualitative agreement between experiment and theory is satisfactory in case of argon as a target but relatively poor when neon is used as a target gas.

1. *Introduction.* The energy loss per unit of distance suffered by an ion moving through a solid, is generally divided into a part due to elastic interactions (nuclear stopping power S_v) and a part due to inelastic interactions of the projectile with the electrons of the solid (electronic stopping power S_e). The latter quantity shows a remarkably oscillating dependence on the atomic number of the projectile Z_1, and the target atom Z_2[1–7]). Neither the theory of Lindhard and Scharff[8]), which describes the stopping as the slowing down in an electron gas, nor the theory of Firsov, which is a friction-like model, predict these oscillations.

As the oscillations were thought to be due to atomic shell-structure effects, it seemed most promising to modify the Firsov theory, because in this theory the inelastic energy loss is given as a function of the impact parameter. Instead of the statistical Thomas–Fermi model for the atom, which was used in the original paper by Firsov, several authors introduced Hartree–Fock electronic wave functions to account for the variations in electron density as a function of the distance to the nucleus[10–14]).

Calculations were then performed along the same line as those of Firsov. The

Q values obtained by these calculations were integrated over an impact-parameter region and yielded electronic stopping-power values which fitted the experimental values surprisingly well. These experimental values were obtained by a measurement of the total stopping power from which an estimated value of the nuclear part is subtracted.

A more direct test of the modified Firsov theory is possible by comparison with the results of single-collision small-angle scattering experiments. In this case the impact parameter is known from the scattering angle and no integration of the calculated Q values over an impact-parameter region is needed. One of the assumptions of the Firsov theory is that the orbit is rectilinear; this means experimentally that only small scattering angles are allowed.

2. *Apparatus.* The experimental setup is schematically shown in fig. 1. Two different accelerators are used, one operating between 30 and 200 keV and the other below 30 keV[15]). The first one is equipped with a sputter ion source[16]) which furnishes ions of both solids and gases. The low-energy ion-beam machine has a uno plasmatron ion source. The beam passes through three aligned apertures. The first two, *a* and *b*, collimate the beam within 5′. The third diaphragm, *c*, has two functions. In the first place it prevents the ions which are reflected at diaphragm *b* from entering the analyser. Secondly it is used as a pumping impedance between the cylinder C, and the rest of the collision chamber. This small cylinder is evacuated with a high pumping speed. With this construction the primary ions travel in high vacuum until a few mm before the scattering centre, so that they are not neutralized. A target gas is introduced into the scattering chamber which is continuously pumped by a liquid-nitrogen baffled mercury diffusion pump. The pumping speed is reduced to about 10 l/s in order to achieve a uniform gas-density distribution during the scattering experiments. The pressure is measured with an ionization gauge of the Bayard–Alpert type. It is calibrated by means of the continuous-flow method[17]), within an absolute accuracy of 2%.

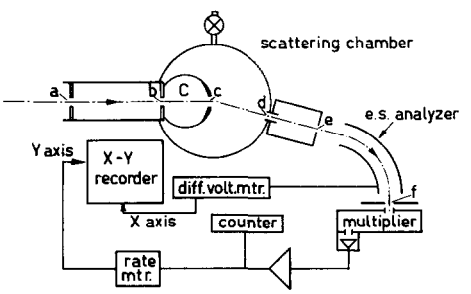

Fig. 1. A schematic diagram of the experimental setup used for the determinations of inelastic energy losses of scattered ions by one collision. $a = b = 0.5$ mm, $d = e = 0.2$ mm, $f =$ from 0 to 2 mm.

The scattered ions pass through two diaphragms, d and e, which in combination with the angular spread in the primary beam define the angular resolution (see 4.1.). The aperture e is the entrance slit of the analyser. The analyser exit slit, f, is adjustable from 0 to 2 mm within an accuracy of 0.01 mm. Under optimal condition the energy resolution of the analyser, $\Delta E/E$, is 4×10^{-4}. Further details of accelerators, scattering chamber and analyser can be found elsewhere[18,19]). The ions which have passed the analyser are counted by means of a Bendix multiplier, coupled to a preamplifier and a main amplifier with pulse shaper. The counting signal is transferred *via* a rate meter to the Y axis of an X–Y recorder. The X input of this recorder is connected to a differential voltmeter reading the analyser voltage with a precision better than 10^{-4}.

3. *Experimental method.* For inelastic collisions, application of the conservation laws of energy and momentum show that measurement of the kinetic energy E_1 of the scattered particles and the scattering angle θ_1, is sufficient to calculate the inelastic energy loss, Q, which is dissipated in this collision:

$$Q/E_0 = 2\gamma\,(E_1/E_0)^{\frac{1}{2}} \cos\theta_1 - (1 + \gamma)\,(E_1/E_0) - \gamma + 1, \tag{1}$$

where E_0 is the primary energy and $\gamma = (M_1/M_2)$, the mass ratio of the colliding particles. In this equation any momentum carried off by ejected electrons has been neglected. Furthermore it is assumed that the target atoms are at rest.

We measure the voltage on the analyser plates which is applied to get the scattered ions through the analyser. This voltage is proportional to the energy of the scattered projectiles, that are transmitted through the analyser:

$$V_1 = cE_1. \tag{2a}$$

At a scattering angle of 0 degrees, while there is no target gas in the collision chamber, we measure the voltage, V_0, which is proportional to the energy of the primary ions:

$$V_0 = cE_0. \tag{2b}$$

Combination of (2a) and (2b) yields:

$$E_1/E_0 = V_1/V_0, \tag{2c}$$

and the theoretical relation (1) goes over into the experimental relation:

$$Q/E_0 = 2\gamma\,(V_1/V_0)^{\frac{1}{2}} \cos\theta_1 - (1 + \gamma)\,(V_1/V_0) - \gamma + 1. \tag{3}$$

3.1. Error analysis. Considering the uncertainties in the individual terms of eq. (3) we get the maximal uncertainty in Q/E_0:

$$\Delta(Q/E_0) = \left|\frac{\mathrm{d}(Q/E_0)}{\mathrm{d}V_1}\right| \Delta V_1 + \left|\frac{\mathrm{d}(Q/E_0)}{\mathrm{d}V}\right| \Delta V_0 + \left|\frac{\mathrm{d}(Q/E_0)}{\mathrm{d}\cos\theta_1}\right| \Delta\cos\theta_1. \quad (4a)$$

For small scattering angles θ_1, the factors $\cos\theta_1$ and V_1/V_0 can be approximated by 1. This yields:

$$\Delta Q = \frac{E_0}{V_0}(\Delta V_1 + \Delta V_0) + 2\gamma E_0 \Delta\cos\theta_1 + \frac{\Delta E_0}{E_0} Q. \quad (4b)$$

In each series of measurements we determine V_0 before and after each plot. If the drift is $(\Delta V_0/V_0) > 2 \times 10^{-4}$ we reject the result; otherwise the V_0, used in the analysis of the plot with the help of formula (3), is found by averaging the two values before and after the measurement. So the relative error in V_0 is less than 10^{-4}. The experimental uncertainty in θ_1 is 3', which results in an error in $\cos\theta_1$ less than 3×10^{-5} in our angular range. The estimated error in V_1 is $\Delta V_1/V_1$ $(\approx \Delta V_1/V_0) = 3 \times 10^{-5}$. The uncertainty $\Delta E_0/E_0$, that is the accuracy with which the primary beam energy is calibrated, is better than 0.3%; the product $(\Delta E_0/E_0)\, Q$ can, compared to the other terms in (4b), be neglected. All together this gives the following result:

$$\Delta Q < (13 + 6\gamma) \times 10^{-5} \times E_0. \quad (5)$$

As an example we calculated the maximum error which can be expected in the case where neon is bombarded with 40 keV Ar^+ ions. The maximum error to be expected is $\Delta Q < 10$ eV. The measured Q value in this case was 25 eV and this value did reproduce within 6 eV.

4. *Widths in inelastic energy-loss peaks.* The observed peak width in the Q spectra is caused by several contributions:

1) the angular spread of the incoming and the scattered beam caused by the finite apertures of the collimators;
2) the limited energy resolution of the analyser caused by the finite apertures of the slits;
3) a spread in the energy of the particles of the incoming beam (acceleration voltage and ion-source instabilities);
4) thermal motion of the target atoms;
5) natural peak width.

4.1. Instrumental effects. 4.1.1. Angular spread. The collimating diaphragms for the primary beam are 0.5 mm and their separation is 690 mm.

Therefore the number of projectiles entering the collision chamber at an angle θ_i with respect to the initial beam direction can be given as in fig. 2a, assuming that the first diaphragm operates as a uniform source of particles. In fig. 2b is shown the probability that a scattered particle, moving at an angle $(\theta_u - \theta_1)$ with respect to the main axis of the analyser, will enter the analyser. The angle between

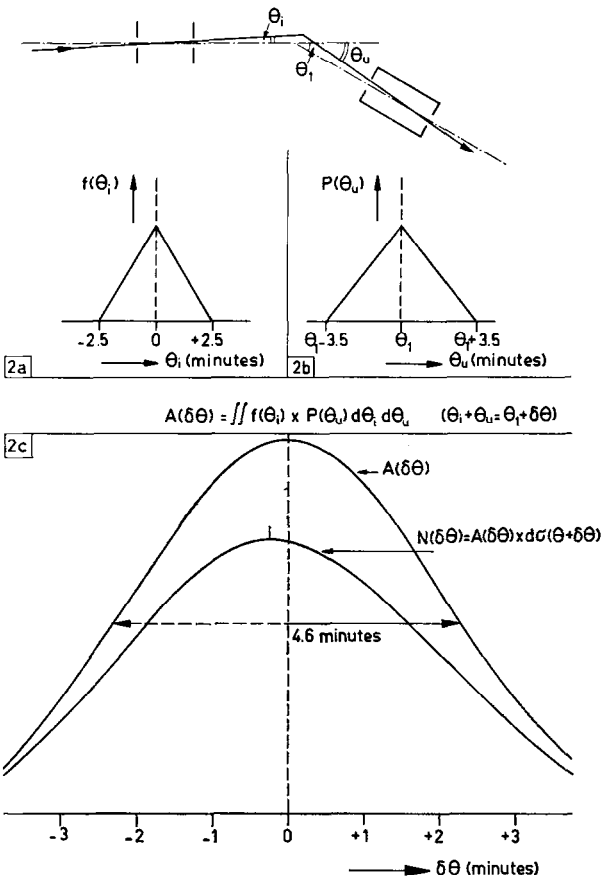

Fig. 2. a) The distribution of primary particles which enter the scattering chamber through an angle θ_i. The ultimate divergence is 2.5′; b) The probability function that particles moving through an angle θ_u enter the analyser. θ_1 is the scattering-angle setting. The ultimate divergence is 3.5′; c) The distribution of scattering angles [$A(\delta\theta)$] and the number of particles which are scattered [$N(\delta\theta)$] as a function of $\delta\theta$, observed at a given scattering-angle setting.

this main axis and the incoming beam direction is the set value of the scattering angle θ_1. The distribution of scattering angles observed at this set angle is calculated by means of the integral:

$$A(\delta\theta) = \iint f(\theta_i)\, P(\theta_u)\, \mathrm{d}\theta_i\, \mathrm{d}\theta_u, \tag{6}$$

with the condition that $\theta_i + \theta_u = \theta_1 + \delta\theta$. The result is shown in fig. 2c. The full width at half maximum is $4.6' = \Delta\theta_1$. To obtain the number of particles which are scattered into the analyser as a function of $\delta\theta$ for a given set angle θ_1 we have to multiply the distribution by the differential cross section. As an example this is done for 60 keV $Ar^+ \rightarrow Ne$ for $\theta_1 = 15'$. In fig. 2c it can be seen that [due to the small variation of $\sigma(\delta\theta)$] the FWHM is not changed and only the most probable scattering angle is 15'' off from the set value. The effect of this spread in scattering angles $\Delta\theta_1$ around a given set angle θ_1, is a spread in the observed secondary kinetic energies of the scattered particles. It causes a broadening of the peak in the spectrum. Assuming that the inelastic energy does not vary over the very small scattering-angle range of $[\theta_1 - \frac{1}{2}\Delta\theta_1, \theta_1 + \frac{1}{2}\Delta\theta_1]$, then the following relation holds:

$$dq = \left[\left(\frac{\partial q}{\partial \theta_1}\right) + \left(\frac{\partial q}{\partial t_1}\right)\left(\frac{\partial t_1}{\partial \theta_1}\right)\right] d\theta_1 = 0, \tag{7}$$

where $q = Q/E_0$ and $t_1 = E_1/E_0$. It follows from (7) that:

$$(\partial t_1/\partial\theta_1) = -(\partial q/\partial\theta_1)/(\partial q/\partial t_1), \tag{8}$$

and the spread in observed kinetic energies is:

$$\Delta t_1 = -(\partial q/\partial\theta_1)/(\partial q/\partial t_1)\,\Delta\theta_1 = \frac{(2t_1 \sin\theta_1)}{\{\cos\theta_1 - [(1+\gamma)/\gamma]\, t_1^{\frac{1}{2}}\}}\,\Delta\theta_1. \tag{9a}$$

The spread Δt_1 causes an apparent spread in q:

$$\Delta q = \left(\frac{\partial q}{\partial t_1}\right)\Delta t_1,$$

so:

$$\Delta q = -(\partial q/\partial\theta_1)\,\Delta\theta_1 = 2\gamma t_1^{\frac{1}{2}} \sin\theta_1 \Delta\theta_1, \tag{9b}$$

which for small scattering angles θ_1 reduces to

$$\Delta q = \Delta t_1 = 2\gamma \sin\theta_1 \Delta\theta_1. \tag{10}$$

For $\gamma = 1$ and $\theta = 1°$ the spread in kinetic energy is $\Delta t_1 = 4 \times 10^{-5}$. This is in most of the cases an order of magnitude smaller than the energy resolution (see next paragraph) of the analyser.

4.1.2. The energy resolution of the analyser. A monoenergetic beam passing through the entrance diaphragm of our analyser is imaged as a line with a width equal to the diameter of this diaphragm on the exit slit. By changing the

voltage on the plates this line moves over the slit. The distribution of detected particles as a function of the analyser voltage is a trapezium or a triangle. So the form of the monoenergetic line is a trapezium (in the case that the exit slit is the largest) or a triangle (if the entrance diaphragm is the largest). The full width at half maximum of these lines corresponds to a relative energy spread of an ideal analyser given by:

$$\Delta E/E = \max(e, f)/272, \tag{11}$$

in which $\max(e,f)$ is the maximum of the widths of entrance diaphragm and exit slit; 272 is a geometrical factor dependent on the radius of curvature of the analyser and the deflection angle[20]). With $\max(e,f) = 0.20$ mm, the relative spread Δt_1 is in the order of 7×10^{-4}. Taking into account that we use a circular entrance diaphragm instead of a rectangular slit, as is assumed in the determination of the geometrical factor, Δt_1 reduces to 5×10^{-4}. For small angles $(\partial q/\partial t_1) = -1$ so $\Delta q = \Delta t_1 = 5 \times 10^{-4}$.

4.1.3. Energy spread of the incoming beam. The incoming beam has a certain energy spread, due to small instabilities of the high voltage and to changing source conditions. Together with the energy resolution of the analyser it causes a finite linewidth of the primary beam. If we analyze this primary beam (at $\theta = 0$) experimentally its linewidth $\Delta E/E$ is found to be of the order of 4×10^{-4}. This is even smaller than the calculated energy resolution of the analyser alone. (This can be due to a very small misalignment such that the primary beam does not completely fill the entrance diaphragm of the analyser which then virtually has a smaller diameter; this effect is only important for $\theta = 0$.) It can be concluded that the energy spread in the primary beam is small.

4.2. Physical effects. 4.2.1. Broadening due to thermal target motion. If the target gas has an absolute temperature T and the velocity of the target atoms is Boltzmann-distributed then application of the conservation laws of energy and momentum yields in first approximation:

$$\overline{\Delta Q^2} = 2kTE_2, \tag{12}$$

[for the derivation of (12) see the appendix].
The full width at half maximum for $T = 300$ K is then given by:

$$\Delta Q \approx 10\,[E_2(\text{keV})]^{\frac{1}{2}}\ \text{eV}. \tag{13}$$

As an example the thermal broadening for 56 keV $Fe^+ \rightarrow Ne$ scattered over 1°23′ was calculated. It was found that $\Delta Q_T = 3$ eV. This is very small compared to the broadening due to the energy resolution of the analyser of 28 eV. In our experiments in general the broadening due to the thermal motion of the target atoms is negligible.

4.2.2. Natural peak width. In the preceding paragraphs we have discussed all the distributions which cause a broadening of a line in the energy spectrum of the scattered projectiles. However, the situation is much more complicated. Recent experiments in the lower primary velocity range[21]) have shown that the total peak is composed of several closely spaced lines each corresponding to excitation of a discrete excited state in one or both collision partners. For one distance of closest approach and one relative velocity a series of discrete inelastic energy losses is found. The energy resolution of our analyser is not high enough to resolve these lines at the primary energies which we used for the present paper. Therefore we observe in general one continuous peak. The width of it is determined by energy distance between the lowest and highest unresolved Q line, the broadening due to thermal motion and instrumental effects. Assuming that the unresolved lines within the peak are gaussian-distributed, one obtains:

$$\Delta Q^2_{\text{observed}} = \Delta E^2 + \Delta Q^2_{\text{thermal}} + \Delta Q^2_{\text{instrumental}}, \tag{14}$$

in which ΔE is the FWHM of the distribution of discrete inelastic energy losses. This equation is used in 5.2 to calculate the ΔE, which quantity is correlated to the range of accessible excitation channels.

5. *Results.* 5.1. Inelastic energy losses as a function of the atomic number of the projectile. Peaks of a number of scattered primary ions with atomic numbers in the range $6 < Z_1 < 29$ were recorded. The velocity of the primary particles was the same for all the cases; the energy in keV was chosen equal to the mass number. The scattering angles were chosen such that the distance of closest approach for all cases was in the order of 0.6 Å. The relation between

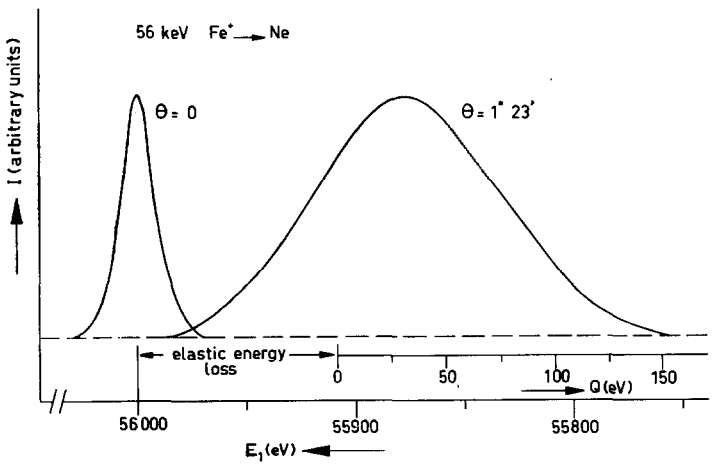

Fig. 3. An example of the secondary energy spectrum of Fe ions scattered over 1°23′ by neon. The spectrum of the primary beam ($\theta = 0$) is used for calibration.

the scattering angles and the distances of closest approach was obtained using a Born–Mayer potential[22]). Neon and argon were used as target gases. An example of a spectrum recorded for 56 keV $Fe^+ \rightarrow Ne$ is shown in fig. 3. The peak recorded is symmetric. This is generally the case for Z_1 numbers > 13. The average value of Q coincides in that case with the value at the maximum of the peak. If the peak is asymmetric, the arithmetic mean value of Q at half-maximum height

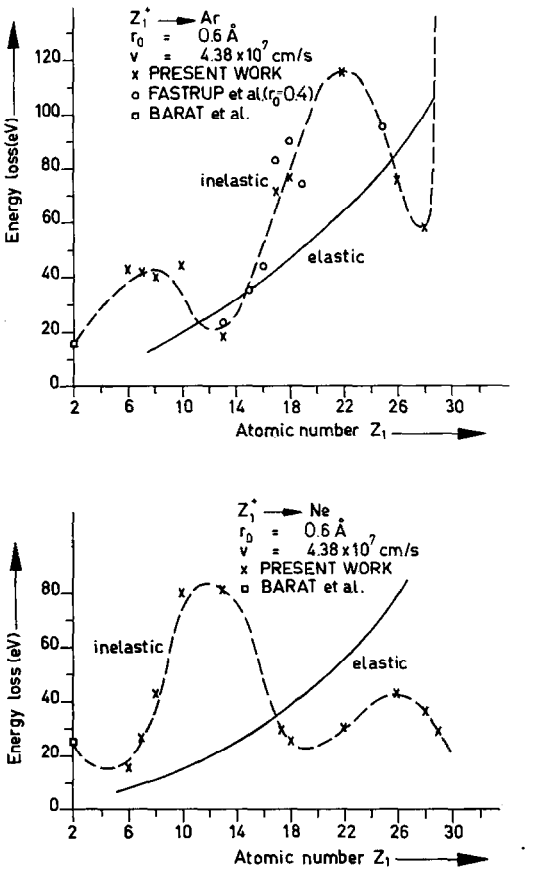

Fig. 4. Inelastic- and elastic-energy losses of different ions passing argon and neon at a distance of closest approach of 0.60 Å with a velocity of 4.38 × 10^7 cm/s. The value of Barat *et al.* was taken from J. Phys. B: Atom. molec. Phys. 3 (1970) 207.

is taken. This introduces an error smaller than 10%. However, for Z_1 numbers < 13 structure is observed. The average value of Q is then obtained by determining the weighted sum of the different components of the peak. In figs. 4 and 5, the inelastic-energy losses are shown as functions of the atomic number of the projectile using neon and argon targets, respectively. The elastic energy loss, defined as the difference between the total energy loss and the inelastic energy

loss, is also given. In fig. 4 the distance of closest approach is 0.60 Å while in fig. 5 the same plots are given for a distance of closest approach of 0.65 Å. The figures show that there is a large shift between argon and neon data. For both argon and neon the minima and maxima are independent on the distance of closest approach in this internuclear-distance range. This roughly holds also with regard to the inelastic energy losses, with exception of the values of argon for Z numbers larger than 22. Here a drastic decrease of the Q values with increasing r_0 is found.

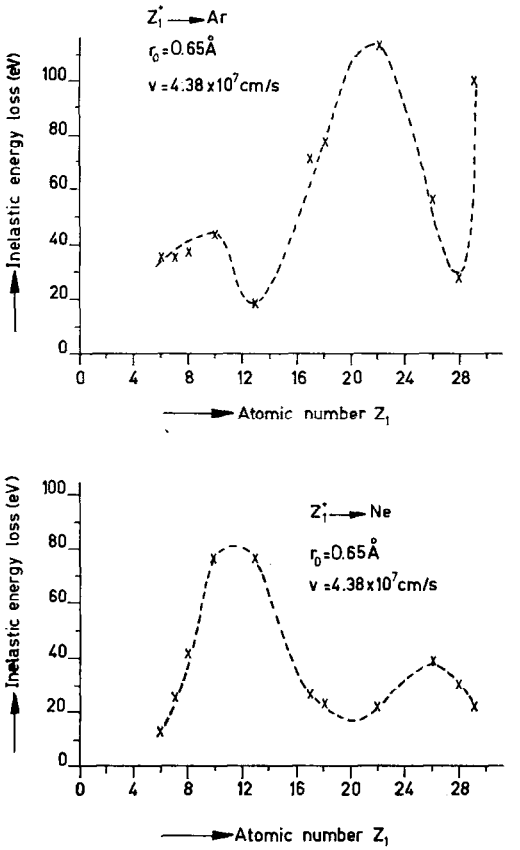

Fig. 5. Inelastic energy losses of different primary ions passing argon and neon at a distance of closest approach of 0.65 Å.

A possible explanation is that for these projectile–target pairs new subshells are penetrated at a distance of around 0.6 Å, while for the other pairs no significant variation in overlap of shells takes place in this region of closest approach. This could also explain why the Q values obtained by Fastrup *et al.*[23]), which are measured at another distance of closest approach (0.4 Å, calculated with the

Lens–Jensen potential), fit with our results for $Z_1 < 22$ in the case of an argon target. To use these values we have corrected for the velocity assuming that Q is proportional to the velocity.

5.2. Spread in inelastic energy as a function of atomic number of the projectile. As was discussed in 4.4., the Q peak is thought to be built up by a number of lines, each of them corresponding to a discrete excitation channel. The energy distance between these lines is too small to resolve them. From high-resolution measurements in the low primary energy region, it is known that the lines, which are then partly resolved, are mostly distributed in a gaussian way.

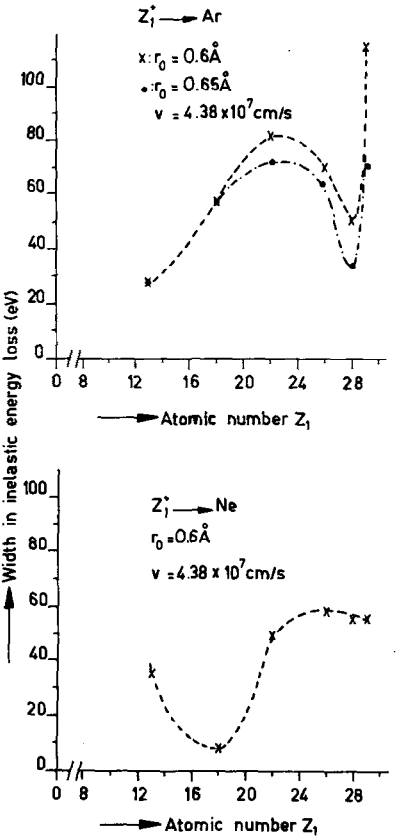

Fig. 6. "Energy range of accessible excitation channels" for collision processes where different primary ions are scattered from argon and neon at two different distances of closest approach.

Then we are allowed to use eq. (14), in calculating ΔE, the FWHM of this distribution.

In fig. 6 these values are plotted against the atomic number of the projectile for two distances of closest approach. It can be seen that ΔE shows the same

oscillations as Q. This indicates, generally speaking, that if the inelastic energy loss is high a large number of excitation channels in a large energy region contribute to this inelastic loss.

6. *Theory.* The original Firsov model[9]) of the inelastic energy loss has been modified by Bhalla, Bradford and Reese[14]) to include the shell structure of the atoms. The modified Firsov model is described in detail elsewhere[14]). Here we summarize the essential features. This model is appropriate for small angles of deflection for which cases the impact parameter and the distance of closest approach are about the same; this is the case for the experimental data presented in this paper. The basic assumption of the Firsov model is that when electrons of one atom come under the influence of the attractive potential of the second atom, there is a momentum transfer equal to mv. The mass of the electron is m and the relative velocity of the projectile with respect to the target atom is v. A plane surface, which is assumed to be located at equal distance from the line of centers of the two atoms, divides the region of attractive potentials of the two atoms. The energy transfer, Q, for an impact parameter, b, is then obtained by calculating the contributions of the electronic flux across the surface of the plane and integrating over the path of the projectile.

$$Q(r_0) = mv \int_{-\infty}^{\infty} \mathrm{d}x \oint_S \Phi \, \mathrm{d}S. \tag{15}$$

The total electronic flux, Φ, has contributions from the projectile and the target atoms. The flux due to the ith shell is given by

$$\Phi_i = (\tfrac{1}{4}) \, |\psi_i|^2 \, w_i \bar{v}_i, \tag{16}$$

where ψ_i is the radial wave function and w_i is the number of electrons in that shell. The average speed of the electron is defined by

$$\bar{v}_i = \langle v_i^2 \rangle^{\frac{1}{2}} = \left[\frac{2}{m} \langle T_i \rangle \right]^{\frac{1}{2}}, \tag{17}$$

where $\langle T_i \rangle$ is the average kinetic energy of the electron. The Hartree–Fock–Slater atomic model was used in the present calculations. Further, the contributions of electrons in the outer shells were included.

The theoretical results of Q are compared with the experimental values in fig. 7a for argon and in fig. 7b for neon. In both these figures, the inelastic energy loss is divided by the dimensionless quantity, v/v_0, which is the ratio of the ion velocity and the Bohr velocity. It should be also noted that Q is in atomic units (1 a.u. = 27.2 eV). The quantity $Q\,(r_0)/(v/v_0)$ is expected to be in-

dependent of v when $v/v_0 \leq 1$ and for large values of r_0. To exhibit the dependence of the inelastic energy loss on r_0, the theoretical values are plotted for two values of the distance of closest approach, r_0.

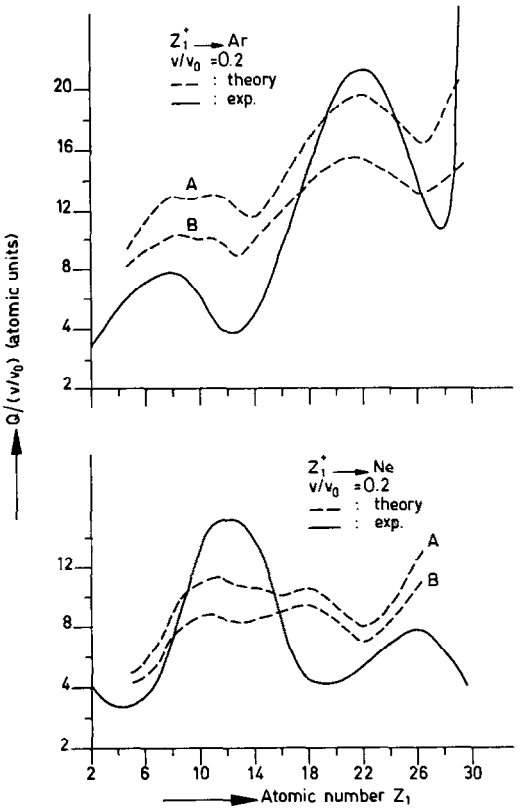

Fig. 7. Theoretical calculations of Q compared with the experimental values obtained at $r_0 = 0.60$ Å. The distances of closest approach used in the calculations were: argon A: 0.65 Å, B: 0.86 Å; neon A: 0.61 Å, B: 0.71 Å.

7. *Discussion.* The experimental inelastic energy loss values and the ones calculated on the basis of the modified Firsov theory show reasonable agreement in the cases where argon is used as a target. The maxima and minima are at about the same Z_1 values. The experimental curve shows a more pronounced structure than the theoretical one. However, we have to bear in mind that the experiments only show that part of the collision processes in which the projectile stays singly ionized after the collision. Processes in which neutralization occurs are not measured by our electrostatic analyser while the theory does not discriminate against the kind of excitation process.

In the case of neon, however, the agreement between theory and experiment is relatively poor, in particular for $Z_1 > 26$ where the experimental values decrease while the theoretical values increase with increasing Z_1. No reason can be mentioned why the theory should hold in the case of argon and breaks down in the case of neon. Both targets have 6 electrons in the outer shell and in both cases the velocity of the projectiles is much less than the orbital velocity of the electrons. Nevertheless the poor agreement in the case of neon suggests that the theory for the description of these inelastic collisions must be reviewed.

Recent measurements[21]) of inelastic energy losses with higher resolution have shown that the total inelastic energy loss mostly can be attributed to discrete excitation processes in target and projectile. Each of these excitation processes has a certain probability to occur as a function of the distance of closest approach and relative velocity of the collision partners. Fano and Lichten[24]) have proposed a model for inner-shell excitation which also might be helpful to describe outer-shell excitation processes, although Lichten in a more recent paper[25]) doubts whether the model, without any changes, is applicable for these cases. At every moment during the collision the electron levels in the pseudomolecule are considered. There are critical internuclear distances, R_c, at which crossings of the levels occur. Transitions of electrons to an unfilled level at a crossing can leave a promoted electron stranded in a higher level after the collision. The probability for such a transition is given by the well known Landau–Zener formula $P = 2p(1-p)$ with $p = \mathrm{e}^{-2\pi H^2/\hbar v(\mathrm{d}E/\mathrm{d}R)}$; here H is the interaction energy between the two states, v is the radial collision velocity and E is the energy splitting between the unperturbed states. Calculation of these transition probabilities as functions of the impact parameter and v should yield the mean inelastic energy loss. This seems certainly the most fundamental approach to the problem.

It is remarkable that the modified Firsov theory which has essentially a statistical nature, predicts at least partly the inelastic energy losses, which are caused by discrete clean atomic processes. However, there is a link between the two approaches, because the promotion in outer shells has also a statistical background. Let us, for example, consider the collisions:

$$\mathrm{Ne}^+ + \mathrm{Ar} \rightarrow \mathrm{Ne}^{+*}(2\mathrm{p}^4, \mathrm{n}l) + \mathrm{Ar}.$$

In terms of the Fano–Lichten model this means that a 2p electron is promoted to an n level. However, there are very many n states, all leading to inelastic energy losses of about 35 eV. So the probability of a Q of 35 eV will largely be determined in a statistical way by the number of crossings. This number of crossings is in first approximation correlated to the electron densities in the different subshells which forms the link to the modified Firsov theory.

Not only the number of crossings is an important parameter but also the probability for an electron to get into the other atomic orbital. In the Fano–Lichten

model crossings do not inevitably lead to a promotion but in the Firsov model, once you have the electron flux from one particle to the other, inelastic energy loss will occur. Therefore the simultaneous observation of unexcited and excited particles in our experiments (for $Z_1 < 13$) is in favour of the Fano–Lichten model and might explain why the experimental average Q values in these cases are lower than the values calculated with the help of the Firsov theory in the case of argon.

From inner-shell excitation studies it is found that the occurrence of crossings is critically linked to the atomic number. For instance it was observed that inner-shell excitation took place only in the lightest of the two collision partners[23]). Recently several authors[26]) have investigated the behaviour of the crossings as a function of Z. A further exploration of this behaviour especially for outer-shell levels might reveal the reason why in the case of neon the modified Firsov theory fails to predict the experimental values.

Acknowledgements. We wish to thank Professor J. Kistemaker, Professor J. Los, Dr. F. J. de Heer and Dr. W. F. van der Weg for their comments and discussions.

This work is part of the research programme of the Stichting voor Fundamenteel Onderzoek der Materie (Foundation for Fundamental Research on Matter) and was made possible by financial support from the Nederlandse Organisatie voor Zuiver-Wetenschappelijk Onderzoek (Netherlands Organization for the Advancement of Pure Research).

APPENDIX

Broadening due to thermal target motion. Assuming that the target particle has the relative momentum $\boldsymbol{p}_T/\boldsymbol{p}_0 = \boldsymbol{\varepsilon}$ ($\varepsilon_x = p_x/p_0$, $\varepsilon_y = p_y/p_0$, $\varepsilon_z = p_z/p_0$; p_0 is the momentum of the primary particle), the conservation of momentum and energy yields the equations:

$$t_2^{\frac{1}{2}} \cos\phi_2 \cos\theta_2 = \gamma^{\frac{1}{2}}(1 + \varepsilon_x) - (\gamma t_1)^{\frac{1}{2}} \cos\phi_1 \cos\theta_1, \tag{A.1a}$$

$$t_2^{\frac{1}{2}} \cos\phi_2 \sin\theta_2 = \gamma^{\frac{1}{2}}\varepsilon_y - (\gamma t_1)^{\frac{1}{2}} \cos\phi_1 \sin\theta_1, \tag{A.1b}$$

$$t_2^{\frac{1}{2}} \sin\phi_2 = \gamma^{\frac{1}{2}}\varepsilon_z - (\gamma t_1^{\frac{1}{2}}) \sin\phi_1, \tag{A.1c}$$

$$1 + \gamma\varepsilon^2 = t_1 + t_2 + q, \tag{A.2}$$

where

$$t_1 = E_1/E_0, \qquad t_2 = E_2/E_0, \qquad q = Q/E_0, \qquad \gamma = M_1/M_2,$$

θ_1 and θ_2 are the scattering angles of projectile and target particle in the X–Y plane (the plane in which the collision is described if $\varepsilon = 0$). ϕ_1 and ϕ_2 are the scattering angles of projectile and target particle in a plane through the Z axis and v_i. The initial beam direction is along the X axis. Quadrature and addition of (A.1a), (A.1b) and (A.1c) yields:

$$t_2 = \gamma\,((1 + \varepsilon_x)^2 + \varepsilon_y^2 + \varepsilon_z^2 + t_1 - 2t_1^{\frac{1}{2}}\{\varepsilon_z \sin\phi_1 + [(1 + \varepsilon_x)\cos\theta_1 + \varepsilon_y \sin\theta_1]\cos\phi_1\}) \tag{A.3}$$

Combination with eq. (A.2) gives:

$$q = 1 - (1 + \gamma)\,t_1 + 2\gamma t_1^{\frac{1}{2}}\{\varepsilon_z \sin\phi_1 + \cos\phi_1\,[(1 + \varepsilon_x)\cos\theta_1 + \varepsilon_y \sin\theta_1]\} - \gamma\,(1 + 2\varepsilon_x). \tag{A.4}$$

For $\varepsilon = 0$ this equation reduces to eq. (1). The thermal target motion causes a certain spread in t_1, Δt_1, and thus, following eq. (1), an apparent spread in q:

$$\Delta q = \left(\frac{\partial q}{\partial t_1}\right)\Delta t_1. \tag{A.5}$$

To find the spread in t_1 due to ε_x, ε_y and ε_z, we have to expand the function $t_1 = t_1\,(\varepsilon_x, \varepsilon_y, \varepsilon_z)$ in a Taylor series:

$$\Delta t_1 = \sum_{i=x,y,z} \varepsilon_i \left(\frac{\partial t_1}{\partial \varepsilon_i}\right) + \sum_{i,j=x,y,z} \tfrac{1}{2}\varepsilon_i\varepsilon_j \left(\frac{\partial^2 t_1}{\partial\varepsilon_i \partial\varepsilon_j}\right) + \cdots. \tag{A.6}$$

In first approximation we do not take into account the second and higher-order terms originating from the Taylor series because $\varepsilon \ll 1$.

The factor $(\partial t_1/\partial\varepsilon_i)$ can be found by differentiation of eq. (A.4):

$$\mathrm{d}q = 0 = \sum_{i=x,y,z} \left(\frac{\partial q}{\partial t_1}\frac{\partial t_1}{\partial \varepsilon_i} + \frac{\partial q}{\partial \varepsilon_i}\right)\mathrm{d}\varepsilon_i, \tag{A.7}$$

giving:

$$\frac{\partial t_1}{\partial \varepsilon_i} = -\frac{\partial q/\partial\varepsilon_i}{\partial q/\partial t_1}. \tag{A.8}$$

Introduction of eq. (A.8) into eq. (A.6) and of eq. (A.6) into eq. (A.5), yields:

$$\Delta q = -\sum_{i=x,y,z} \left(\frac{\partial q}{\partial \varepsilon_i}\right)\varepsilon_i. \tag{A.9}$$

The broadening of q lines due to thermal target motion is then given by:

$$\overline{\Delta q^2} = \sum_{i=x,y,z} \left(\frac{\partial q}{\partial \varepsilon_i}\right)^2 \overline{\varepsilon_i^2}, \tag{A.10}$$

because $\overline{\varepsilon_i \varepsilon_j} = 0$ if $i \neq j$ as the ε_i are independent stochastic variables.

If the target gas has an absolute temperature T and the velocity is Boltzmann-distributed we find:

$$\overline{\varepsilon_x^2} = \overline{\varepsilon_y^2} = \overline{\varepsilon_z^2} = \frac{\frac{1}{2}m_2\overline{v_T^2}}{\frac{1}{2}m_1 v_0^2} \frac{m_i}{m_1} = \frac{\frac{1}{2}kT}{\gamma E_0}. \tag{A.11}$$

From eqs. (A.4) and (A.11) we get for eq. (A.10):

$$\overline{\Delta q^2} = 4\gamma^2 \{1 + t_1 - 2t_1^{\frac{1}{2}} \cos\phi_1 \cos\theta_1\} \tfrac{1}{2}kT/\gamma E_0, \tag{A.12}$$

which can be approximated by [see eq. (A.3) with $\varepsilon_i = 0$]:

$$\overline{\Delta q^2} = 4t_2 (\tfrac{1}{2}kT/E_0).$$

So

$$\overline{\Delta Q^2} = 2kTE_2.$$

For $T = 300$ K this yields:

$$\Delta Q = 7\ [E_2(\text{keV})]^{\frac{1}{2}}\ \text{eV}.$$

At half-maximum height we find:

$$\Delta Q = 10\ [E_2(\text{keV})]^{\frac{1}{2}}\ \text{eV}. \tag{A.13}$$

REFERENCES

1) Ormrod, J.H. and Duckworth, H.E., Canad. J. Phys. **41** (1963) 1424.
2) Ormrod, J.H., MacDonald, J.R. and Duckworth, H.E., Canad. J. Phys. **43** (1965) 275.
3) MacDonald, J.R., Ormrod, J.H. and Duckworth, H.E., Z. Naturforsch. **21a** (1966) 130.
4) Fastrup, B., Hvelplund, P. and Sautter, C.A., Mat. Fys. Medd. Dansk. Vid. Selsk. **35** (1966) 10; Hvelplund, P. and Fastrup, B., Phys. Rev. **165** (1968) 408.
5) White, W. and Mueller, R.M., Phys. Rev. **187** (1969) 499.
6) Eriksson, L., Davies, J.A. and Jespergaard, P., Phys. Rev. **161** (1967) 219.
7) Eisen, F.H., Canad. J. Phys. **46** (1968) 561.
8) Lindhard, J. and Scharff, M., Phys. Rev. **124** (1961) 128.
9) Firsov, O.B., Zh. eksp. teor. Fiz. **36** (1959) 1517; Soviet Physics-JETP **9** (1959) 1076.
10) Bhalla, C.P. and Bradford, J.N., Phys. Letters **27A** (1968) 318.
11) Winterbon, K.B., Canad. J. Phys. **46** (1968) 2429.

12) Cheshire, I.M., Dearnally, G. and Poate, J.M., Phys. Letters **27A** (1968) 304; Proc. Roy. Soc. **A 311** (1969) 47.
13) Cheshire, I.M. and Poate, J.M., Proc. Int. Conf. At. Coll. Phen. in Solids (1969) 351.
14) Bhalla, C.P., Bradford, J.N. and Reese, G., Proc. Int. Conf. At. Coll. Phen. in Solids (1969) 361.
15) Van Eck, J., De Heer, F.J. and Kistemaker, J., Physica **30** (1964) 1171.
16) Hill, K.J. and Nelson, R.S., Nuclear Instrum. and Meth. **38** (1965) 15.
17) Bannenberg, J.G. and Tip, A., Proc. of the 4th Int. Vac. Congress Manchester (1968).
18) Wolterbeek Muller, L. and De Heer, F.J., Physica **48** (1970) 345.
19) Snoek, C., thesis, Amsterdam (1966).
20) Ewald, H. and Hintenberger, H., Meth. Anw. Mass. Weinheim (1953) 69.
21) Bierman, D.J. and Turkenburg, W.C., Physica, to be published.
22) Abrahamson, A.A., Phys. Rev. **178** (1969) 76.
23) Fastrup, B., Hermann, G. and Smith, K.J., Phys. Rev. **3** (1971) 1591.
24) Fano, U. and Lichten, W., Phys. Rev. Letters **14** (1965) 627.
25) Lichten, W., Phys. Rev. **164** (1967) 131.
26) Barat, M. and Lichten, W., private communication.